Cell

RNA-Methylation-Dependent RNA Processing Controls the Speed of the Circadian Clock

Jean-Michel Fustin,[1] Masao Doi,[1] Yoshiaki Yamaguchi,[1] Hayashi Hida,[1] Shinichi Nishimura,[2] Minoru Yoshida,[3] Takayuki Isagawa,[4] Masaki Suimye Morioka,[4] Hideaki Kakeya,[2] Ichiro Manabe,[4] and Hitoshi Okamura[1,*]

[1]Graduate School of Pharmaceutical Sciences, Department of System Biology, Kyoto University, 46-29 Yoshida-Shimo-Adachi-cho, Sakyo-ku, Kyoto 606-8501, Japan

[2]Graduate School of Pharmaceutical Sciences, Department of System Chemotherapy and Molecular Sciences, Kyoto University, 46-29 Yoshida-Shimo-Adachi-cho, Sakyo-ku, Kyoto 606-8501, Japan

[3]Chemical Genetics Laboratory, RIKEN, Hirosawa 2-1, Wako, Saitama 351-0198, Japan

[4]The University of Tokyo, Graduate School of Medicine, Department of Cardiovascular Medicine, 7-3-1 Hongo, Bunkyo, Tokyo 113-8655, Japan

*Correspondence: okamurah@pharm.kyoto-u.ac.jp

http://dx.doi.org/10.1016/j.cell.2013.10.026

SUMMARY

The eukaryotic biological clock involves a negative transcription-translation feedback loop in which clock genes regulate their own transcription and that of output genes of metabolic significance. While around 10% of the liver transcriptome is rhythmic, only about a fifth is driven by de novo transcription, indicating mRNA processing is a major circadian component. Here, we report that inhibition of transmethylation reactions elongates the circadian period. RNA sequencing then reveals methylation inhibition causes widespread changes in the transcription of the RNA processing machinery, associated with m^6A-RNA methylation. We identify m^6A sites on many clock gene transcripts and show that specific inhibition of m^6A methylation by silencing of the m^6A methylase *Mettl3* is sufficient to elicit circadian period elongation and RNA processing delay. Analysis of the circadian nucleocytoplasmic distribution of clock genes *Per2* and *Arntl* then revealed an uncoupling between steady-state pre-mRNA and cytoplasmic mRNA rhythms when m^6A methylation is inhibited.

INTRODUCTION

The mammalian circadian clock regulates metabolism mainly via transcriptional control of clock output genes coding for master metabolic switches or rate-limiting enzymes. Metabolism in turn can adjust the clock, for example by modulating acetylation/deacetylation of histones on promoters activated by core clock protein complex CLOCK:ARNTL (Nakahata et al., 2008) or directly by affecting acetylation status of PER proteins (Asher et al., 2008).

(De)acetylations, however, are only one of many possible biochemical modifications that have the potential to link the circadian clock with metabolism. Here, we focused on transmethylations, i.e., the addition of only one carbon ($-CH_3$) to target substrates. Unlike acetylation that only affects proteins, transmethylations are found at each step of the central dogma: DNA methylation, RNA methylation, and protein methylation (histone and nonhistone) have all been described (Carmel and Jacobsen, 2001). The role of histone methylation for the function of the circadian clock in mammals has recently been investigated (Katada and Sassone-Corsi, 2010; Valekunja et al., 2013; Vollmers et al., 2012). Similarly, the significance of the less dynamic DNA CpG methylation for circadian clock inactivation during the development of cancer and other diseases has been suggested (Ripperger and Merrow, 2011). In contrast, the role of nonhistone protein methylation and RNA methylation is unknown.

It has been known for many years that about 10% of genes are rhythmic in the liver, driven by the circadian clock (Akhtar et al., 2002). More recent RNA-sequencing data have shown that, of these rhythmic genes, only about a fifth is driven by de novo transcription (Koike et al., 2012). This observation has put regulation of splicing and RNA processing at the forefront of biology since it is not only significant for the function of the clock itself but also how it regulates metabolism. In this light, RNA-methylation-dependent RNA processing appears to be an interesting avenue.

All transmethylations, to various degrees, are influenced by the metabolic state of the cell due to their sensitivity to the availability of S-adenosylmethionine (SAM), the universal methyl donor cosubstrate, and to the relative amount of the its by-product, S-adenosylhomocysteine (SAH), that acts as a competitive inhibitor (Carmel and Jacobsen, 2001). The SAM/SAH ratio is known as the "methylation potential." Investigations into cellular transmethylations have relied on the pharmacological inhibition of SAH hydrolysis (Chiang, 1998). This inhibition leads to the accumulation of SAH, the decrease of the methylation potential, and ultimately to the inhibition of transmethylations.

To our knowledge, this approach has never been applied to the investigation of which transmethylations are needed for the circadian clock function. Here, we report that the mammalian circadian clock is exquisitely sensitive to the biochemical inhibition

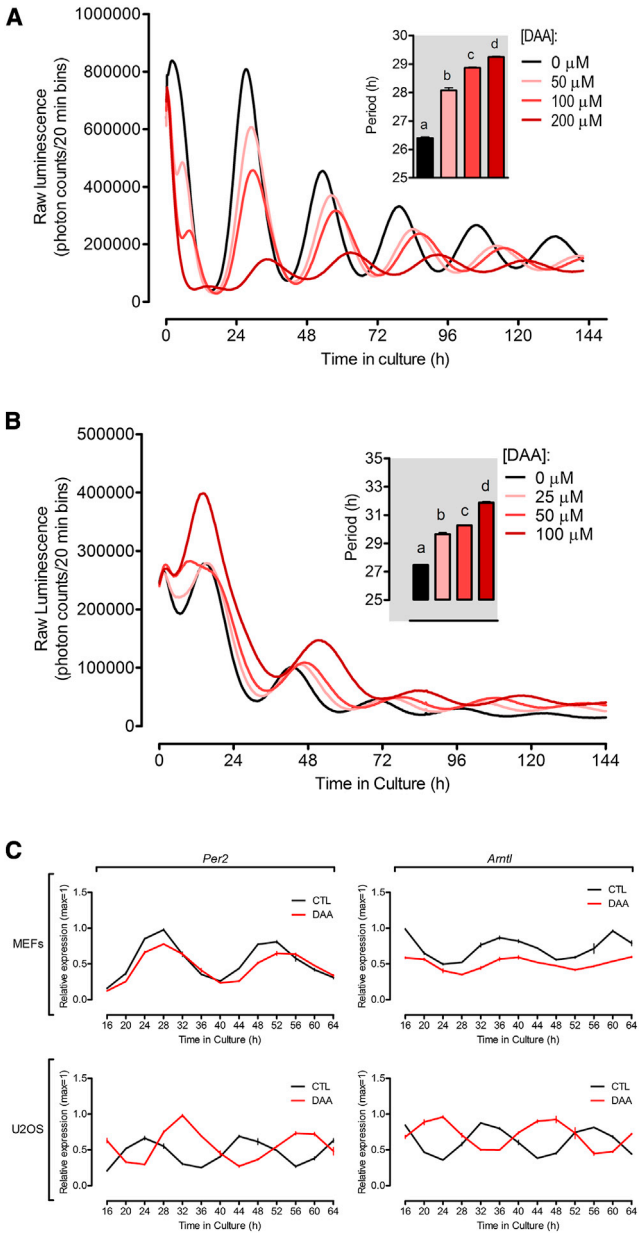

Figure 1. Global Methylation Inhibition Elongates the Circadian Period in Peripheral Cell Types

(A) DAA dose dependently increases the period of PER2::LUC MEF. Traces show mean of n = 2 dishes. Insert shows period analyzed by one-way ANOVA and Bonferroni post hoc test, all significance $p < 0.001$ (mean ± SD, n = 2).

(B) Same observations in human U2OS cells stably transfected with an Arntl-luc reporter. Traces show mean of n = 2 dishes. Insert shows period analyzed by one-way ANOVA and Bonferroni post hoc test, all significance $p < 0.01$ (mean ± SD, n = 2).

(C) MEFs and or U2OS cells were treated with 100 μM DAA or vehicle, *Arntl* and *Per2* gene expression was measured every 4 hr starting from 16 hr post-DAA. Note the similar pattern obtained with luciferase reporters. Data show mean ± SEM of n = 3 replicate dishes. See also Figure S1 and Table S2.

of transmethylations, with the period length being inversely proportional to the methylation potential. We discover in parallel that transcriptional regulation of RNA processing machinery is the main response to the global inhibition of transmethylations. Focusing then on RNA processing, we reveal that specific inhibition of m^6A-RNA methylation by knockdown of the methyltransferase *Mettl3* is sufficient to elicit circadian period elongation due to a decrease in RNA processing efficiency. The importance of RNA-methylation-dependent RNA processing for the circadian clock is then further demonstrated by inhibiting m^7G-cap methylation and subsequent cap-binding complex association, which also leads to period elongation. We therefore revealed the importance of epitranscriptomic regulation of the circadian clock.

RESULTS

Transmethylation Inhibition by 3-Deazaadenosine Elongates the Circadian Period in Peripheral Cell Types

One of the most potent and frequently used SAH hydrolysis inhibitor is 3-deazaadenosine (DAA) (Chiang, 1998). We first tested the effect of DAA on embryonic fibroblasts prepared from mice (MEF) carrying a heterozygote fusion between the core clock protein PER2 and luciferase (PER2::LUC, Figure 1A) and in human U2OS cells stably transfected with an Arntl-luc reporter (Figure 1B). A dramatic increase of SAH induced by DAA, without effect on methionine or S-adenosylmethionine, was confirmed with PER2::LUC MEFs (Figure S1A available online). In both cell types, DAA led to the elongation of the circadian period. The expression of *Per2* and *Arntl* measured directly was affected by DAA in a manner consistent with real-time luminescence data (Figure 1C). DAA dampened oscillations in MEF but not in U2OS. No dramatic effects were observed on cell viability or proliferation, and the cells recovered completely from the influence of DAA upon a medium change (Figures S1B, S1C, and S1D). Period elongation in both cell types was also obtained with deazaneplanocin A (DZnepA), a nonmetaboliseable carbocyclic SAH hydrolysis inhibitor analog of DAA, confirming a mechanism dependent on methylation inhibition (Figure S1E). This demonstrates that the mammalian circadian clock in peripheral cell types is sensitive to the methylation potential collapse.

Transmethylation Inhibition Elongates the Locomotor Activity Rhythm Period

To investigate whether the master mammalian circadian clock that resides in the hypothalamic suprachiasmatic nucleus (SCN) is also sensitive to global methylation inhibition, we treated organotypic SCN slices prepared from Per1-luc reporter mice with DAA (Figure 2A). In this system as well, DAA significantly elongated the circadian period, suggesting a mechanism conserved in both peripheral and master clocks.

Since the SCN controls rhythmic locomotor activity, we tested DAA in mice by direct infusion into the third ventricle, above the SCN, and recorded locomotor activity. Mice showed a significant elongation of the activity rhythm period during DAA infusion compared to controls (CTL, 23.80 ± 0.08 hr; DAA, 24.88 ± 0.45 hr; $p < 0.01$ in Bonferroni post hoc test after significant two-way ANOVA; Figure 2B). This effect was reversible, disappearing after the delivery duration of the minipumps used (~2 weeks).

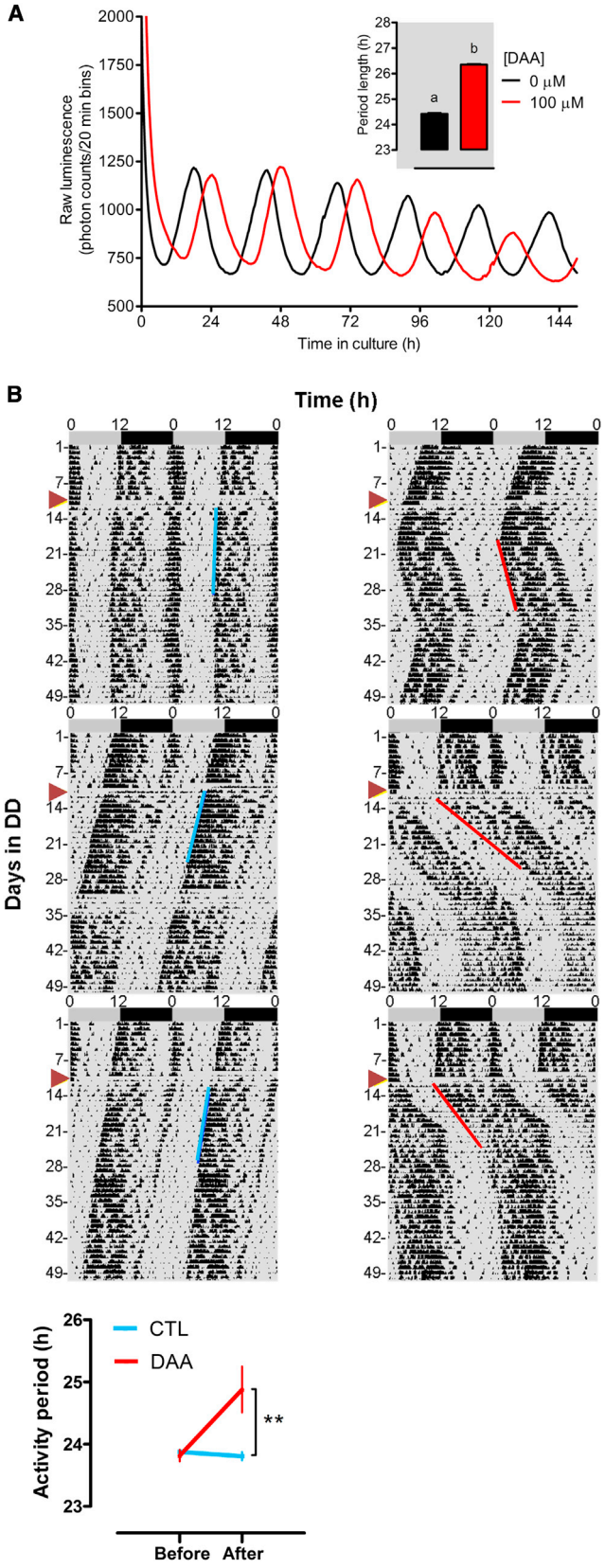

Figure 2. The Circadian Master Clock in the Brain Is Sensitive to Transmethylation Inhibition

(A) DAA increases the period of Per1-luc SCN slices. One representative slice for CTL and DAA treatment is shown. Insert shows period analysis, a versus b $p < 0.001$ in t test, n = 3, mean ± SEM.

(B) Brain DAA infusion (mice operated on the day indicated by brown triangles) increases the locomotor activity rhythm period. Graph on the bottom: mean ± SEM, analyzed in two-way ANOVA/Bonferroni analysis of n = 3 animals, with ** = $p < 0.01$. DD = constant darkness.

Transcriptional Regulation of RNA Processing Machinery Is a Major Response to DAA

To gain an insight into the mechanisms underlying period elongation, we treated U2OS cells with DAA or vehicle for 24 hr to avoid any potential acute effect of DAA, then analyzed the transcriptome by RNA sequencing (Figure 3A). A total of 236,890 transcripts corresponding to 25,865 unique gene IDs were detected. After filtering, 4,360 and 5,120 unique gene IDs were respectively induced and inhibited by DAA (Figure 3B). DAA had a complex effect on gene expression, since 9,480 genes among 12,120 were significantly regulated. Gene ontology (GO) analysis on the entire list of 9,480 single gene IDs, ranked according to their p values, resulted in many nonspecific hits (Figure 3C and Table S1). Interestingly, the 4th most significant hit with highest Enrichment values (>8) was "rhythmic process," containing clock-related genes such *Per1*, *Per3*, *Dbp*, *Tef*, and *Bhlhe41* (Table S1). This suggests that the circadian clock is among the systems most sensitive to methylation inhibition, but due to the breadth of the response to DAA this analysis did not provide any mechanistic insights.

We then separately analyzed the 4,360 induced and the 5,120 repressed genes against the 9,480 significantly regulated genes as background. The induced group showed an uncanny enrichment in RNA metabolic processes (Figure 3C and Table S1). The most significant match, RNA processing (GO:0006396), is described as "any process involved in the conversion of one or more primary RNA transcripts into one or more mature RNA molecules." Among genes induced by DAA our data set included in this GO term are, notably, the RNA m^{7}G-cap methylases *Rnmt* and *Rnmt1l*, as well as the m$^{2'\text{-}O}$ribose-cap methyltransferase *Ftsjd2*; the m^{6}A demethylase *Alkbh5*; other RNA methylases such as *Mettl2a*, *Mettl2b*, and *Rrp8*; adenosine deaminases such as *Adar* and *Adat1*; many other RNA-binding proteins such as *Ncbp2* and *Rbms1*; splicing factors such as *Sf3a1* and *Sf3a2*. The repressed gene group showed significant enrichments mainly (three out of four) in processes related to translation due to many ribosomal proteins and translation initiation factors among downregulated genes (Figure 3C and Table S1). Together this suggests that the transcriptional program of the RNA processing machinery reacts to the global methylation inhibition by DAA, maybe in an attempt to correct a deficient RNA-methylation-dependent processing. Supporting this hypothesis, RNA methyltransferases are known to be the most sensitive to the decrease of the methyl potential (Carmel and Jacobsen, 2001). In particular, DAA is a strong inhibitor of the internal N^6-Methyladenosine (m^{6}A) (Backlund et al., 1986). Since the circadian clock involves a transcription feedback loop, period elongation via RNA-methylation-dependent RNA processing mechanisms would be a thought-provoking and novel possibility.

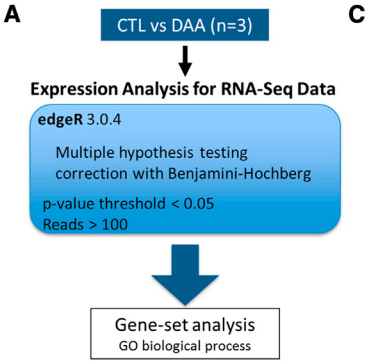

C

GO Term	Description	P-value	FDR q-value	Enrichment
GO:0016339	calcium-dependent cell-cell adhesion	2.54E-10	4.01E-07	7.89
GO:0007416	synapse assembly	4.17E-10	5.64E-07	8.86
GO:0048742	regulation of skeletal muscle fiber development	6.06E-07	2.39E-04	9.03
GO:0048511	**rhythmic process**	**9.29E-06**	**1.57E-03**	**8.75**

GO Term	Description	P-value	FDR q-value	Enrichment
GO:0006396	RNA processing	1.02E-09	9.70E-06	1.3
GO:0016070	RNA metabolic process	1.40E-08	6.65E-05	1.13
GO:0034470	ncRNA processing	4.74E-07	1.50E-03	1.42
GO:0034660	ncRNA metabolic process	2.02E-06	2.13E-03	1.34

GO Term	Description	P-value	FDR q-value	Enrichment
GO:0019083	viral transcription	3.68E-14	3.49E-10	1.74
GO:0000278	mitotic cell cycle	2.52E-13	1.20E-09	1.39
GO:0006414	translational elongation	3.57E-13	1.13E-09	1.67
GO:0006614	SRP-dependent cotranslational protein targeting to membrane	1.73E-12	2.73E-09	1.63

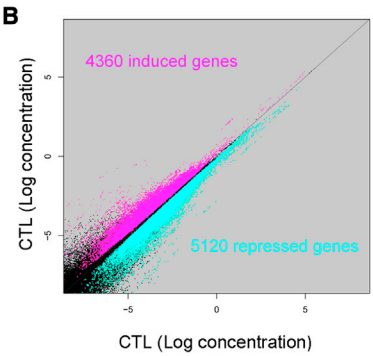

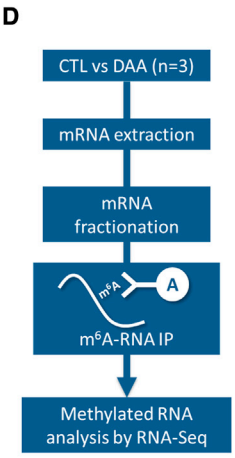

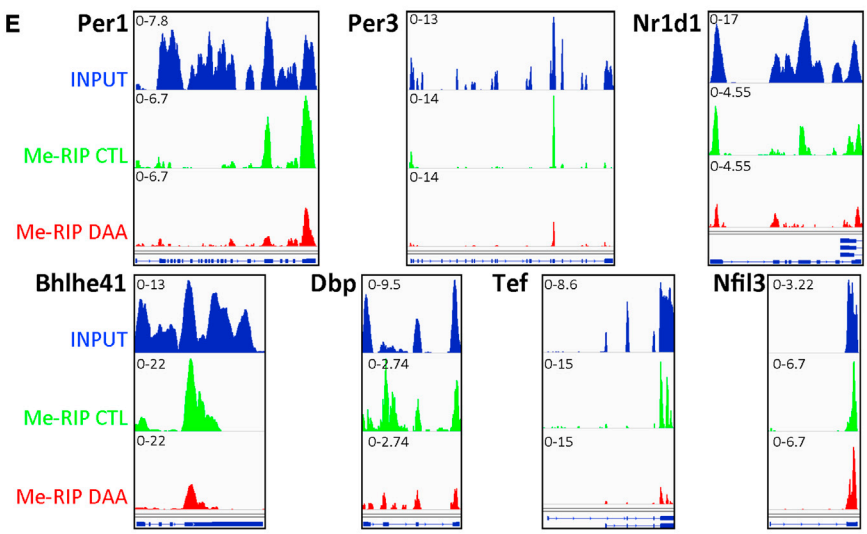

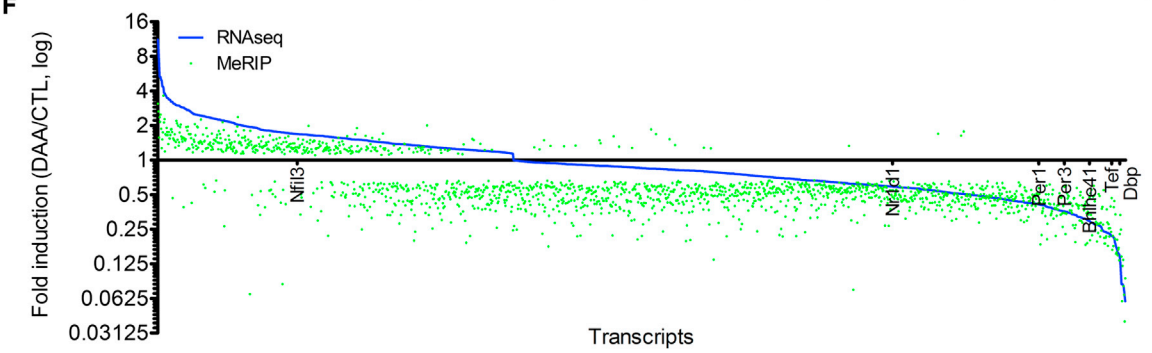

(legend on next page)

Me-RIP Sequencing in U2OS Shows Transcriptome-wide m^{6}A Inhibition

To provide genome-wide information on which m^{6}A methylation sites in which transcripts are affected by DAA, the fragmented mRNA from U2OS cells used above was used as input for RNA immunoprecipitation with an anti-m^{6}A antibody (Me-RIP, Figure 3D). Our data revealed pervasive inhibition of m^{6}A methylation, since 2,293 transcripts from single gene IDs were significantly regulated, containing 78% (1,789) of decreased transcripts, as opposed to only 54% in the input. *Per1*, *Per2, Per3, Dbp, Nr1d1*, and *Nr1d2* transcripts show major methylation sites near the 3′ end and in their longest internal exon, confirming the pattern of m^{6}A enrichment reported before (Dominissini et al., 2012; Meyer et al., 2012). m^{6}A sites were also detected in the 3′ regions of *Clock*, *Nfil3*, *Tef*, *Bhlhe40*, and *Bhlhe41*, and in the 5′ region of *Arntl*, *Nr1d1*, and *Per3* (Figure S2). Significant ($p < 0.05$) decrease in m^{6}A methylation was detected for *Per1*, *Per3*, *Tef*, *Dbp*, *Nfil3*, *Bhlhe41*, and *Nr1d1* (Figure 3E).

The 504 transcripts with increased methylated peaks under DAA treatment may appear startling, but 373 of these 504 transcripts were also induced in the input. Plotting the fold induction of all common 1,779 transcripts showing significant DAA/CTL variations in the Me-RIP and the input revealed that transcripts induced by DAA in the input consistently have a lower fold-induction ratio in the Me-RIP. This indicates DAA induces the transcription of these genes but inhibits m^{6}A methylation of their mRNA (Figure 3F). In contrast, transcripts that are repressed by DAA (<0.70-fold) in the input show correlated variations in the Me-RIP.

DAA Treatment of MEFs Inhibits m^{6}A Methylation and Slows RNA Processing

The RNA-seq experiments above were performed with U2OS cells, to allow comparison with other human cells (Dominissini et al., 2012; Meyer et al., 2012). To investigate the consequent mechanisms, we decided to shift to MEFs extracted from PER2::LUC reporter mice. These knockin mice carry an insertion of luciferase in phase with exon 23 of the Per2 gene (Yoo et al., 2004), making them invaluable to follow *Per2* mRNA or protein processing in real-time. These cells were shown to respond to DAA similarly to U2OS in Figure 1.

To confirm the inhibition of RNA methylation by DAA in these cells, total RNA extracted from MEFs treated with DAA or vehicle for at least 24 hr was immunoprecipitated with the anti-m^{6}A-RNA antibody. In addition, we also used an anti-m^{7}G-cap-RNA antibody to compare the effect of DAA on this methylation of the cap. Moreover, to investigate the possibility that RNA methylation shows time-dependent variations, we also measured m^{6}A methylation every 4 hr across 24 hr, starting from 24 hr post-DAA. *Per1*, *Per2*, *Dbp*, and *Arntl* transcripts were quantified in the immunoprecipitated (methylated RNA) and supernatant (unmethylated) fractions, and the ratio between the two was calculated (Figure 4A). For these transcripts, the m^{6}A methylated/unmethylated mRNA ratio was significantly lower under DAA, but the m^{7}G-cap methylation ratio was not affected and no consistent time-dependent differences in methylation in these transcripts were detected. While the resistance of m^{7}G-cap methylation to DAA has been previously reported (Backlund et al., 1986), we can't reject the possibility that cotranscriptional cap methylation was also inhibited by DAA, causing uncapped pre-mRNA degradation (Jiao et al., 2013). These results nonetheless demonstrate that steady-state mRNA m^{6}A methylation, but not m^{7}G-cap methylation, was inhibited by DAA in MEFs.

Next, we monitored RNA processing dynamics by pulse-chase total RNA labeling click cytochemistry. MEFs were labeled with ethynyl uridine for 2 hr then washed before treatment with 100 μM DAA or vehicle. DAA delayed RNA processing, as evidenced by the prolonged nuclear labeling intensity (Figure 4B), even when de novo transcription was blocked by actinomycin D (Figure S3A). To confirm these observations with mRNA-specific information, we treated cells with 100 μM DAA or control, then quantified *Arntl* and *Per2* mRNA from the cytoplasmic or nuclear fractions extracted after 0, 2, and 4 hr post-DAA (Figure 4C). These results reveal DAA caused a relative increase in the nuclear mRNA fraction, which was significant for *Arntl* at 2 and 4 hr post-DAA and at 4 hr post-DAA for *Per2*. *Arntl* was very sensitive to DAA since at 2 hr the nuclear mRNA content increased despite a reduction in steady-state pre-mRNA and in cytoplasmic mRNA (Figure S3B). *Arntl* and *Per2* steady-state pre-mRNA levels were both strongly reduced under DAA treatment (Figure 4C). The efficiency of our fractionation was checked by quantifying the levels of a mitochondrial genome-encoded transcript, and by measuring *Per2* pre-mRNA concentration in both fractions (Figure S3B).

It has been reported previously that *Per2* mRNA degradation rate is controlled in a circadian manner and is higher during the waning phase of *Per2* expression (Woo et al., 2009). We therefore surmise that if the period elongation elicited by DAA is indeed caused by slower RNA processing, the delay would occur mostly in the waning of *Per2*. Moreover, to compare the respective effects of DAA on RNA processing and those of the transcriptional elongation inhibitor actinomycin D, we treated

Figure 3. DAA triggers Changes in RNA Processing Machinery and Inhibits m^{6}A-RNA Methylation

(A) Experimental paradigm and methods.

(B) Scatter plot showing the genes significantly induced (pink) or repressed (turquoise) by DAA in the input.

(C) Gene ontology analysis with all transcripts ranked according to p values (top, blue), with only induced genes (middle, pink) or with only repressed genes (bottom, turquoise). FDR = false discovery rate.

(D) Experimental paradigm of Me-RIP.

(E) Transcripts showing significant ($p < 0.05$) decrease in m^{6}A methylated peaks. Blue, input RNA from CTL-treated cells; green, Me-RIP from CTL-treated cells; red, Me-RIP from DAA-treated cells. Scale is provided on the top left of each track.

(F) Significant DAA/CTL-fold inductions of shared 1,779 transcripts between input (blue) and Me-RIP samples (green). Transcripts are sorted along the x axis in decreasing DAA/CTL ratio in the input. Genes induced by DAA in the input have decreased fold-induction in the Me-RIP, while fold induction of genes repressed by DAA correlate in the input and Me-RIP. Note *Dbp*, *Tef, Per1, Per2, Nr1d1*, and *Bhlhe41* among the most downregulated genes both in the input and Me-RIP, consistent with top GO analysis at C. See also Figure S2 and Table S1.

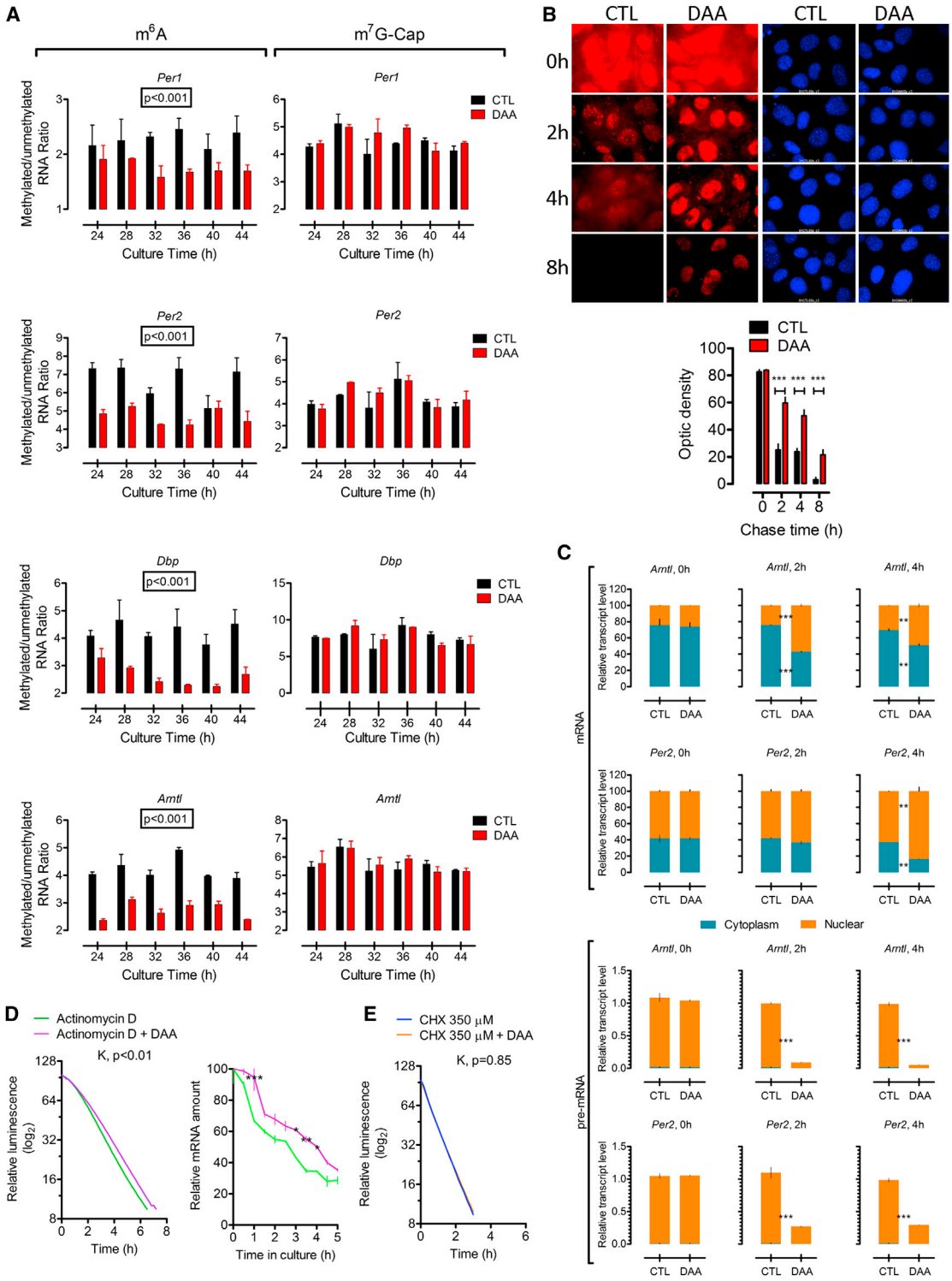

Figure 4. DAA Inhibits Transcription and Delays mRNA Nuclear Export

(A) Treatment of MEFs with 100 μM DAA inhibits m^6A-RNA methylation of all clock gene transcripts investigated (analyzed in two-way ANOVA/Bonferroni, CTL versus DAA $p < 0.001$ for all transcripts) but does not significantly inhibits m^7G-Cap methylation. Mean ± SEM, n = 3 biological replicates. No consistent effect of time or interaction was found.

(B) DAA causes nuclear retention of de novo labeled RNA. Labeling was stopped at time 0 hr, coincidental with the start of DAA treatment (100 μM). Representative pictures of Alexa 594 (red) and Hoechst counterstaining (blue). Note the diffuse cytoplasmic labeling at 4 hr only in CTL-treated cells. Lower graph shows mean intensity of 5 nuclei (±SEM); ***$p < 0.001$ in two-way ANOVA/Bonferroni.

(legend continued on next page)

PER2::LUC MEFs with DAA and/or sub-saturating dose of actinomycin D and recorded luminescence (Figure S3C). As previously reported, mild inhibition of transcription with a low dose of actinomycin D caused circadian period shortening (Dibner et al., 2009). DAA treatment led to opposite results, and cotreatment with both agents showed additive negative effects. Normalization and alignment of traces revealed that DAA and actinomycin D both caused acceleration of the increasing phase of *Per2*, but their effects became opposite during the waning phase (Figure S3D). Taken together, these results show that while DAA can act like a transcription elongation inhibitor, which at least partly explains the decrease in pre-mRNA observed above, its period elongating effect is the dominating component and coincides with *Per2* mRNA processing.

Next, we investigated the half-life of *Per2::luc* mRNA by real-time luminescence assay. PER2::LUC MEFs were first treated with dexamethasone for 2 hr to induce high *Per2::luc* expression, then cells were treated with saturating levels of actinomycin D (5 μM), and luminescence was acquired every 10 min. The results, a significant delay in the half-life of PER2::LUC luminescence, confirmed by direct quantification of *Per2* mRNA, further indicate delayed RNA processing (Figure 4D). Using the translation inhibitor cycloheximide instead of actinomycin D (Figure 4E) confirms DAA does not affect PER2::LUC protein half-life but only that of its mRNA. We next analyzed the half-life of 20 clock-related transcripts and housekeeping genes in U2OS cells treated with actinomycin D with or without DAA, showing that the DAA-dependent stabilization of transcripts is widespread but specific to a subset of genes, with *Arntl*, *Tef*, *Nr1d2*, and *Per3* among the most affected (Figure S4). Together our data suggest delayed mRNA processing leads to period elongation, as was previously predicted by mathematical modeling (Wilkins et al., 2007).

Knockdown and Overexpression of *Mettl3* Have Opposite Consequences on the Circadian Period

The data so far suggest the period elongation depends on the inhibition of m^{6}A RNA-methylation-dependent processing by DAA. To specifically inhibit m^{6}A methylation, we knocked down the expression of *Mettl3,* the SAM-binding subunit of the only known N6-Adenosine-methyltransferase. First confirming the reduction of METTL3 proteins, knockdown of *Mettl3* with either of two different siRNA led to the elongation of the circadian period in both U2OS and MEFs (Figures 5A and 5B). Waveform analysis in PER2::LUC MEFs once more revealed asymmetric period elongation, with a pronounced delay only observed during the waning phase of *Per2* that closely mimics the effects of DAA (Figures S5A and S5B). In contrast to DAA, however, specific m^{6}A inhibition did not cause observable changes during the rising phase, suggesting a mechanism other than m^{6}A methylation accelerates the increase of *Per2* under DAA treatment. No deleterious effects caused by *Mettl3* knockdown were observed on either cell types (Figure S6B), as also confirmed by harmonious and stable oscillations with a comparable baseline.

U2OS cells are known for the responsiveness to siRNA-mediated knockdown (Zhang et al., 2009). We showed U2OS cells are indeed exquisitely sensitive to *Mettl3* knockdown compared to MEFs, showing a 3-hr-period elongation with only 100 pmol of siRNA#48. We then sought to maximize knockdown efficiency in these cells. U2OS cells were transfected with 100 or 250 pmol of siRNA control or #48 and the period was analyzed, showing a proportional increase of period with rising siRNA #48 concentrations (Figure 5C). In addition, the m^{6}A-methylated/unmethylated ratio of *Arntl* transcript was quantified as a marker for functional knockdown (Figure 5C), revealing m^{6}A inhibition by *Mettl3* knockdown causes exponential period elongation.

To investigate the possibility that *Mettl3* overexpression instead leads to period shortening, U2OS Arntl-luc cells were stably transfected with an expression vector for wild-type hMettl3 or a mutated version (Mettl3Δ) bearing D394A and W397A mutations. These mutations are within the universally conserved catalytic motif IV of METTL3, known to severely blunt m^{6}A methylase activity in *Saccharomyces* (Bujnicki et al., 2002; Clancy et al., 2002). Expression of the respective *Mettl3* was first confirmed by sequencing on cDNA isolated from each colony (Figure S5C). As hypothesized, clones expressing the wild-type form showed shorter period length than the control cells expressing Mettl3Δ (Figure 5D).

Knockdown of *Mettl3* Leads to RNA Processing Delay

Can slow m^{6}A-dependent RNA processing cause a slow clock? We tested this hypothesis by first showing that global RNA processing was affected by *Mettl3* silencing. RNA labeling by pulse-chase click cytochemistry revealed a delay in the loss of nuclear RNA label in PER2::LUC MEFs transfected with siRNA#48 compared to control, as was observed with DAA (Figure 6A). Silencing of *Mettl3* caused a delay in nuclear label decay even in the presence of actinomycin D to block transcriptional elongation, directly demonstrating slow RNA processing underlies the results observed (Figure S7). Similar results were obtained in U2OS cells (not shown).

Next, to show the impact of such a slow processing on clock gene expression, *Arntl* and *Per2* were quantified, in the nuclear and cytoplasmic fractions of U2OS cells transfected with 250 pmol of siRNA #48 or control (maximal silencing conditions), every 4 hr for 36 hr (Figure 6B). The results reveal that *Mettl3* knockdown causes a delay in the exit of mature mRNA from

(C) Quantification of *Arntl* and *Per2* mRNA in nuclear and cytoplasmic fractions of CTL/DAA-treated cells after 0, 2, and 4 hr. Bar height represents the contribution of each fraction to total cellular mRNA (100%), all comparisons in two-way ANOVA/Bonferroni; $^{**}p < 0.01$; $^{***}p < 0.001$; mean ± SD, n = 2.

(D) PER2::LUC MEFs were stimulated by dexamethasone for 2 hr, then with 5 μM actinomycin D ± 100 μM DAA immediately before starting measurements. Curves were analyzed by one phase decay exponential fitting and comparing the best fit value for the rate constant K by *F* test (n = 2). Right graph shows similar experiment but *Per2* mRNA was quantified every 30 min by real-time PCR. Data analyzed by two-way ANOVA/Bonferroni, mean ± SEM, n = 3. CTL versus DAA, $^{*}p < 0.05$; $^{**}p < 0.01$; $^{***}p < 0.001$.

(E) Same as D, but using 350 μM cycloheximide (CHX) instead of ActinoD. K was not significant.

See also Figures S3 and S4, and Table S2.

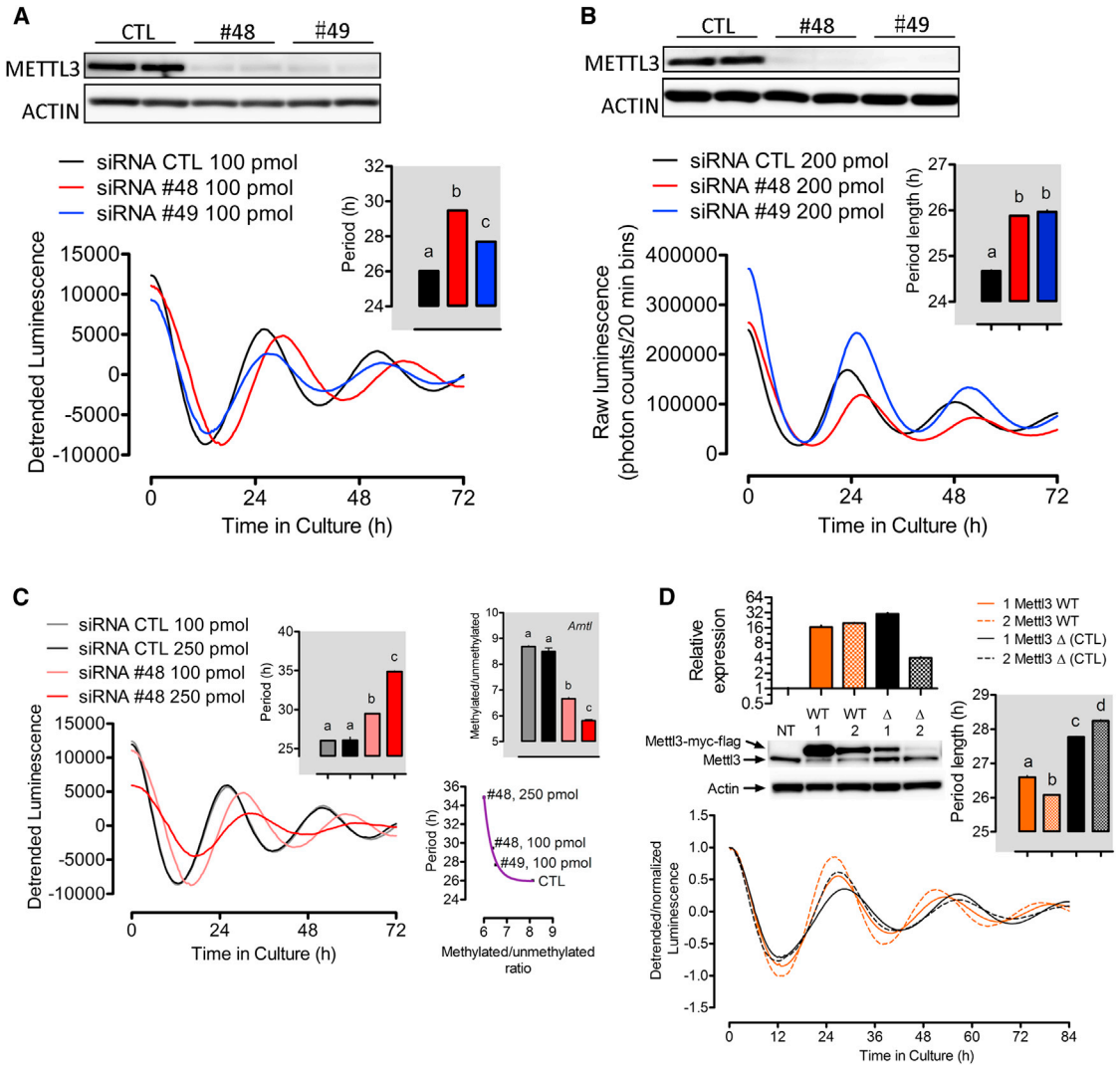

Figure 5. Specific Inhibition of m^{6}A-RNA Methylation Elongates the Circadian Period

(A and B): *Mettl3* knockdown (two different siRNA, #48 and #49) causes period elongation in Arntl-luc U2OS cells (A) and in (B) PER2::LUC MEFs. Traces show mean of n = 2 dishes. Left insert shows period, mean ± SD of n = 2 dishes, analyzed by one-way ANOVA/Bonferroni post hoc, all significance levels at least $p < 0.05$. On the top of each graph, knockdown of METTL3 was confirmed for each cell type.

(C) Increasing the concentration of siRNA#48 dose dependently elongates the circadian period in U2OS cells. The insert shows period analyzed in one-way ANOVA/Bonferroni, all comparison at least $p < 0.01$, mean ± SD, n = 2. Right upper graph shows decreased m^{6}A methylation of *Arntl* transcript under CTL or knockdown conditions, analyzed in one-way ANOVA/Bonferroni, all significant comparison at least $p < 0.01$, mean ± SD, n = 2 biological replicates. Lower right graph shows exponential period elongation when m^{6}A is progressively inhibited.

(D) Overexpression of wild-type METTL3 cause shorter period compared to control conditions when METTL3 is mutated and inactive (Δ). For each colony isolated, top inserts show quantification of total *Mettl3* expression by real-time PCR (expression in nontransfected cells = 1, mean ± SD, n = 2), and detection of native and cloned (myc-flag tagged) METTL3. Right insert shows period analyzed by one-way ANOVA, all comparisons at least $p < 0.05$, mean ± SD, n = 2 for each colony. See also Figures S5 and S6, and Table S2.

the nucleus, detectable at the troughs of both *Per2* and *Arntl* transcripts. For *Arntl*, a normal processing delay of about 4 hr is seen between nuclear steady-state pre-mRNA and cytoplasmic mRNA, but peak cytoplasmic mRNA is further delayed around 4 hr in *Mettl3* knockdown cells. Together these results demonstrate that the lack of m^{6}A-RNA methylation causes a delay in RNA processing, affecting clock gene expression dynamics.

Cap Methylation and Cap Binding Complex Also Regulate the Circadian Period

While the role of m^{6}A-RNA methylation in splicing, mRNA export and translation remains to be clarified, that of 5′ cap methylation and subsequent binding of the Cap-binding complex (CBC) has been extensively studied (Carmody and Wente, 2009). If m^{6}A-RNA-methylation-dependent processing is critical for the circadian clock, we surmise that knockdown of either the m^{7}G-Cap

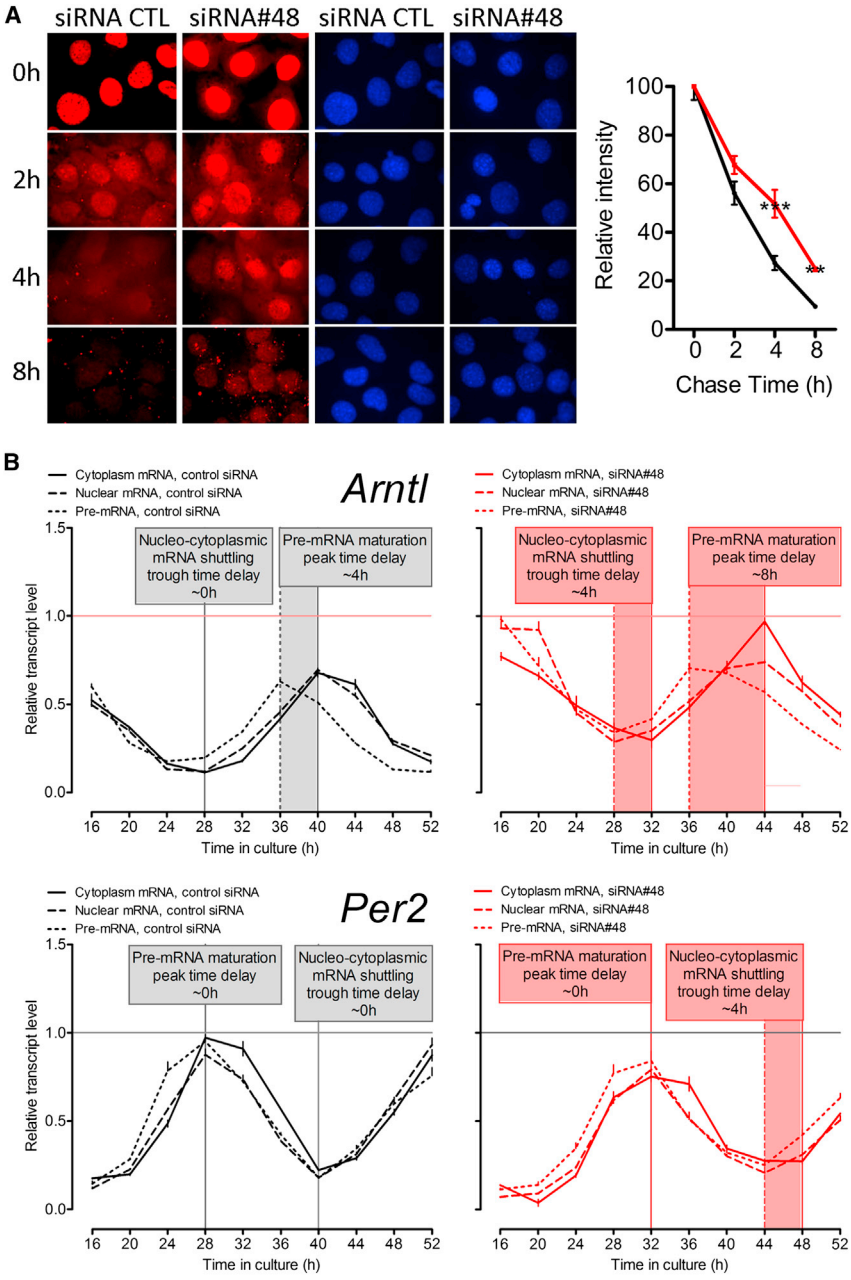

Figure 6. Specific Inhibition of m^{6}A-RNA Methylation Delays mRNA Export and Affects Clock Gene Dynamics

(A) *Mettl3* knockdown by siRNA#48 leads to overall RNA nuclear retention. Representative pictures of Alexa 594 (red) and corresponding Hoechst counterstaining (blue), graph on the right shows relative mean intensity (0 hr = 100 for both CTL and siRNA#48) of five nuclei (±SEM) analyzed by two-way ANOVA/Bonferroni, $^{**}p < 0.01$, $^{***}p < 0.001$.

(B) *Mettl3* knockdown by siRNA#48 causes increased time-lag between *Arntl* pre-mRNA and mature mRNA in the cytoplasm, and increased time-lag between nuclear and cytoplasmic mature *Arntl* and *Per2* mRNA. Notice the synchronous peak and trough times for nuclear and cytoplasmic mRNA for both *Arntl* and *Per2* in CTL cells, but trough cytoplasmic mRNA is delayed in knockdown conditions. For *Arntl*, notice the 4 hr-delay between peak pre-mRNA and mRNA in CTL cells, becoming 4 hr in knockdown conditions. Data show mean ± SEM of n = 3 replicate dishes. See also Figure S7 and Table S2.

methylase *Rnmt* or the main CBC subunit *Ncbp1* would also elongate the circadian period. We first confirmed knockdown of RNMT and NCBP1 proteins (Figure 7A), then demonstrate that silencing of either of these proteins causes a delay in the nuclear RNA labeling decay in a manner similar to that of *Mettl3* (Figure 7B). *Rnmt* or *Ncbp1* silencing led to the circadian period elongation (Figures 7C and 7D), and cosilencing of *Mettl3* with *Rnmt* to inhibit both m^{6}A and m^{7}G-cap methylation revealed additive effects on circadian period length, indicating nonredundant mechanisms (Figure 7E). These results confirm our conclusions made in the previous sections that the circadian clock, composed of a transcription-translation negative feedback loop, is exquisitely sensitive to perturbations in RNA-methylation-dependent RNA processing. Based on our results, we propose RNA methylation regulates a significant portion of the circadian transcription-translation feedback loop (Figure 7F).

DISCUSSION

Here, we established the importance of RNA methylation for the function of the biological clock. More work is needed: while m^{6}A appears RNA sequence specific, m^{7}G-Cap is thought to be ubiquitous, and how these methylations are regulated is unclear. The c-Myc proto-oncogene can regulate the formation of m^{7}G-Cap on many mRNAs (Cowling, 2010), and while it is clear m^{7}G-Cap is necessary for nuclear export and translation, we do not know how gene expression is regulated by *induced* m^{7}G-Cap. Interestingly, c-Myc is an E box (5′-CANNTG-3′)-binding factor like CLOCK:ARNTL that drives circadian transcription. Whether m^{7}G-Cap induction is common to all E-box-binding factor or only to c-Myc remains to be investigated. Similarly, the physiological function of N^6-Methyl-2′-O-methyladenosine methylation of the cap, which is also sensitive to methyl cycle inhibition (Backlund et al., 1986), is unknown, as a reminder that the field of RNA methylation is still in its infancy.

Histone methylation is circadian and modulates circadian transcription (Katada and Sassone-Corsi, 2010; Valekunja et al., 2013; Vollmers et al., 2012) but has not been linked to the circadian period in mammals. As a control, we have investigated whether DAA treatment also inhibits histone methylation

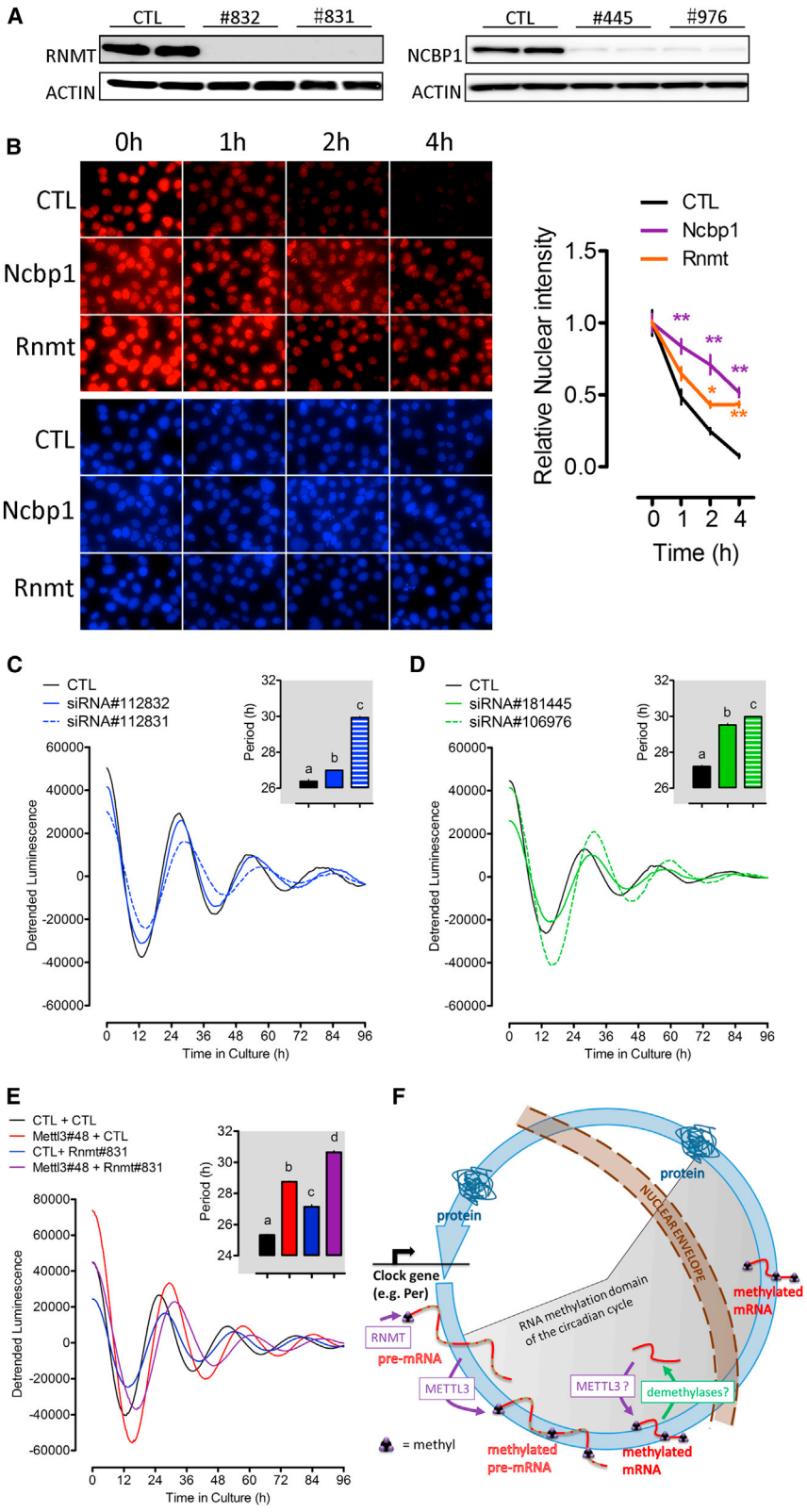

Figure 7. m^{7}G-cap Methylation and the Cap Binding Complex Are Also Required for Clock Function

(A) Effective knockdown of RNMT or NCBP1 proteins in Arntl-luc U2OS cells (100 pmol siRNA/dish).

B: *Rnmt* (#831) or *Ncbp1* (#976) silencing leads to the retention of RNA in the nucleus of Arntl-luc U2OS cells. To prevent de novo transcription during chase, 5 μM actinomycin D was included in the culture medium. Representative pictures of Alexa 594 (red) and corresponding Hoechst counterstaining (blue), graph on the right shows relative mean intensity (0 hr = 1 for CTL, *Rnmt* and *Ncbp1*) of 10 nuclei (±SEM) analyzed by two-way ANOVA/Bonferroni, *$p < 0.05$ **$p < 0.01$.

(C) *Rnmt* knockdown causes period elongation in Arntl-luc U2OS cells. Insert shows period, mean ± SD of n = 2 replicate traces, analyzed by one-way ANOVA/Bonferroni post hoc, all significance levels at least $p < 0.05$.

(D) *Ncbp1* knockdown causes period elongation in Arntl-luc U2OS cells. Insert shows period, mean ± SD of n = 2 replicate traces, analyzed by one-way ANOVA/Bonferroni post hoc, all significance levels at least $p < 0.001$.

(E) Additive effects of *Mettl3* and *Rnmt* cosilencing on circadian period elongation (70 pmol/dish siRNA each, 140 pmol total siRNA for each combination). Left insert shows period, mean ± SD of n = 2 replicate traces, analyzed by one-way ANOVA/Bonferroni post hoc, all significance levels at least $p < 0.01$.

(F) We propose a model in which the circadian cycle, containing processes such as splicing, mRNA nuclear export and translation, is modulated by RNA methylation. It remains unclear whether m^{6}A methylation only occurs at the pre-mRNA level or m^{6}A methylation-demethylation cycles can happen at the mRNA level. See also Figure S6.

and show that lysine methylation of histone H1, H2, and H3, as well as H3K4-trimethylation are all inhibited (Figure S1F). We confirmed *Mettl3* silencing did not inhibit histone methylation, however (Figure S5D). While histone methylation is out of the scope of the present paper, it may be possible that histone methylation inhibition by DAA contribute to the effects of DAA, especially the cell-type-specific changes in amplitude observed.

While we have demonstrated that nuclear export and stability of clock gene mRNA was affected in our studies, precisely what aspect(s) of RNA-methylation-dependent processing cause(s) period elongation remains unclear since splicing, mRNA export, and stability, 3′-end cleavage, polyadenylation, and translation are all interdependent. Tentatively, we tested the splicing inhibitor spliceostatin A (Kaida et al., 2007) on PER2::LUC MEFs. Spliceostatin A somewhat modified PER2::LUC oscillations, but the period did not change significantly, suggesting splicing inhibition per se does not control circadian period (Figure S6A).

Virtually all transmethylations rely on the availability of the universal methyl donor cosubstrate SAM, and the relative amount of SAH that acts as a competitive inhibitor. Cyclic abundance of these two metabolites has been described (Eckel-Mahan et al., 2012; Schalinske and Steele, 1992), which may rhythmically regulate transmethylations (histone and other substrates) within the cell at the metabolic level. In particular, circadian RNA methylation driving gene expression rhythms when de novo transcription is not would provide an elegant explanation to the observations made by Koike and coworkers (Koike et al., 2012). Recently, two m^6A demethylases were identified (Jia et al., 2011; Zheng et al., 2013), supporting the possibility of dynamically regulated m^6A methylation.

We have demonstrated the presence of methylation sites within many clock gene transcripts. Using unfragmented RNA for immunoprecipitation, a method usually used with these anti-methyl-RNA antibodies (Cole and Cowling, 2009; Fernandez-Sanchez et al., 2009), we confirmed these observations. Although the indiscriminate inhibition of m^6A methylation, by DAA or *Mettl3* knockdown, led to circadian period elongation, it would be interesting to investigate specifically which m^6A site, within which clock gene transcript, is sufficient for period elongation. For this matter, Figure 3F provides an interesting insight: some clock genes are among the most inhibited transcripts in our data set. In the canonical circadian clock model based on *Drosophila* work, PER proteins are the main state variables (Rosbash, 1995), also in mammals (Chen et al., 2009). Indeed, a network model of the circadian clock already predicted that all processes reducing the half-life of *Per2* mRNA, including faster mRNA degradation and faster mRNA export, would lead to a shortened period, and slower mRNA export would lead to longer period (Wilkins et al., 2007). Delaying nuclear import of PER2 proteins by deleting its nuclear localization site leads to longer circadian period (Miyazaki et al., 2007), suggesting delayed nuclear export of *Per2* mRNA may have the same consequences. When our data are seen together, however, it appears that *Arntl* is very sensitive to DAA treatment or Mettl3 silencing, more so than *Per2*, with clear nuclear accumulation (Figure 4C), more pronounced delays in transcripts processing (Figure 6B), and markedly elongated half-life (Figure S4), suggesting *Arntl* may contribute to the period elongation observed. Future work should clarify this issue.

In conclusion, we have established the importance of RNA methylation for the function of the circadian clock. This pioneering work provides many potential avenues for further investigations.

EXPERIMENTAL PROCEDURES

Reagents

All chemicals were obtained from Nacalai-Tesque (Japan) unless otherwise stated.

Real-Time Luciferase Assays, Drug Treatment, and Transfection

Cells were plated at around 50% density and allowed to grow for at least 3 days in phenol-red free standard medium. Cells were then synchronized by a medium change, with 200 nM dexamethasone (Sigma-Aldrich) for 2 hr. Medium was then replaced with new medium containing 1 mM luciferine and luminescence was recorded in a luminometer-incubator at 37°C (Kronos DIO, ATTO) in successive bins of 20 min. DAA (Sigma-Aldrich) or vehicle was added to the medium at the appropriate time.

For siRNA transfection, U2OS (stably transfected with *Arntl*-luc reporter) or MEF cells were plated in standard medium. The next day, medium was changed, all antibiotics omitted. Invitrogen Stealth siRNA against human *Mettl3* (#48 and #49), *Rnmt* (#831 and #832), *Ncbp1* (#976 and #445), or negative controls of similar GC% were complexed with Lipofectamine 2000 (Invitrogen) following manufacturer's protocol. For the control in cosilencing of *Rnmt* and *Mettl3*, a 1:1 mix of two different negative controls siRNA was used. Medium was replaced 6 to 8 hr after transfection. Two days later, cells were synchronized with 200 nM dexamethasone. After 2 hr, medium was replaced with medium containing 1 mM luciferine. Luminescence was recorded in successive bins of 20 min at 37°C. Period estimates from luminescence traces were obtained using BRASS (Plautz et al., 1997). Luminescence traces from U2OS Arntl-luc cells were first detrended (subtract a 24-hr-moving average) in order to obtain a more stable baseline before period estimation. Figure S5A illustrates this process. The impact of the silencing of every gene tested here on cell viability and proliferation was briefly assessed before downstream experiments by taking phase-contrast representative pictures of corresponding cell populations (Figure S6B).

For stable transfection of U2OS Arntl-luc cells, cells were transfected with Origene TrueORF hMettl3 vector or the mutated version (obtained by standard PCR) using Lipofectamine 2000 following manufacturer's protocol. Twenty-four hours after transfection medium was changed, adding 1 mg/ml G418 for Neomycin selection, and cells were incubated until colonies had formed. Untransfected cells showed 100% mortality. Colonies were picked and passaged in 35 mm Petri dishes and allowed to grow to confluence in phenol-red free DMEM/F12 containing charcoal-stripped FBS and 1 mg/ml G418 (kept in medium therefater). At confluence, cells were treated 2 hr with 200 nM dexamethasone and luminescence was measured as described above. Circadian period of colonies was confirmed after two additional passages.

Per1-luc SCN Slices Culture

Slices were prepared according to our standard method (Yamaguchi et al., 2000).

Animals and Brain DAA Infusion

All experiments were approved by the animal experimentation committee of Kyoto University. C57/BL6 males were maintained at 23°C ± 1°C with 50% ± 10% relative humidity, one animal per cage on a 12 hr light/12 hr dark cycle (lights on 8:00, lights off 20:00), food and water *ad libitum*. DAA was continuously delivered to the SCN via osmotic pump as described (Doi et al., 2011). In brief, the infusion cannula (Alzet, Brain Infusion Kit 2) was directed stereotaxically to the SCN; the osmotic pump (Alzet, pump model 1002) containing 10 mM DAA (58 nmol/day) was implanted subcutaneously (dorsal skin) by surgery under anesthesia. After surgery, animals were returned to their home cages and maintained under constant darkness.

LCMS-IT-TOF Protocol

The amount of metabolites was measured by LCMS-IT-TOF (Shimadzu, Japan). LC separation was performed on a ZIC-HILIC column (Merck Millipore, Germany; 2.1 × 150 mm, 3.5 μm) at 40°C. MeCN/H2O/formic acid (1:98:1) (A) and MeCN/H2O/formic acid (98:1:1) (B) were used as the mobile phase, with a gradient elution system: 95% B for 1 min, shifted to 10% B in 9 min, and kept 10% B for 2 min. The system was allowed to equilibrate for 10 min at 95% B prior to the next analysis. The flow rate was 100 μl/min. Ten microliters metabolite extract was analyzed and the peak areas of the metabolites detected in a positive ion mode were normalized by the peak areas of the internal standard, Bis-Tris.

Me-RIP-Seq

Total RNA was extracted from cells treated with deazaadenosine (100 μM) or vehicle for 24 hr, n = 3. mRNA samples were purified from 200 microg total RNA by two rounds of Oligotex-dT30 (Takara, Japan). All mRNA samples were analyzed by Bioanalyzer to check for mRNA quality. mRNA was then fragmented using NEBNext Fragmentation Magnesium buffer (NEB Japan) then purified with RNA Minelute column (QIAGEN, Japan). All fragmented mRNA samples were analyzed by Bioanalyzer to confirm a major population of ~200 bp RNA fragments; 500 ng fragmented mRNA from each sample was immunoprecipitated using the anti-m6A antibody, then extracted following the procedure explained below.

Sequencing libraries were prepared using the NEBNext Ultra RNA Library Prep Kit with partially modified steps in random primer annealing condition as 65°C for 15 min, and sequencing was performed on an Illumina Genome Analyzer IIx.

Reads were mapped to the human genome (hg19 from UCSC genome browser database) using TopHat v2.0.0 (Trapnell et al., 2009). Only reads that had a Phred quality score ≥ 25 were analyzed. For filtering rRNA and tRNA, BEDtools package (Quinlan and Hall, 2010) was used with rRNA and tRNA annotations downloaded from UCSC table browser was used.

For evaluating differentially expression between DAA- and CTL-treated U2OS cells, EdgeR (Robinson and Smyth, 2007) was used for statistical testing using trimmed mean of M-values (TMM) method for normalization and generating *P*-values on Genomatix Genome Analyzer (Genomatix, Munich, Germany). For identification and quantification of Me-RIP regions, each value obtained with Me-RIP sample was background-subtracted with corresponding values in the input samples. Only transcripts with #reads > 50 were included in the analysis. Input and Me-RIP data are available in the GEO repository under accession number GSE48037.

Normalized expression value (NE-value) is calculated based on the following formula:

$NE = 10^7 * \text{the number of reads}_{region}/(\text{the number of reads}_{mapped} * \text{length}_{region})$ (Audic and Claverie, 1997).

GO Enrichment Analysis

Transcripts with p value > 0.05, then with #reads < 100 in CTL samples were discarded. GO enrichment analysis was carried out with single gene IDs using GOrilla (Eden et al., 2007; Eden et al., 2009), either using a single ranked list of genes or using two unranked lists (target and background). Redundant GO hits were filtered using REVIGO.

RNA Immunoprecipitation

RNA was first extracted using a combination of Sepasol RNA I super G and RNeasy (QIAGEN, Japan) following RNeasy protocol for Lipid tissues with Sepasol instead of Qiazol. Next, 1.5 μg of RNA or 500 ng fragmented mRNA was incubated in 250 μl of 20% protein A- or G-Agarose slurry in IPP buffer for 1 hr at 4°C for background removal. The RNA/beads slurry was then centrifuged at 700 × *g*, 4°C for 2 min, the RNA supernatant (~200 μl) was used in the next step and the agarose beads pellet discarded.

Fifty percent protein G- or A-Agarose slurry in IPP buffer was conjugated with anti-m^7G-cap mouse monoclonal antibody (Synaptic Systems, 80 μl ascites/ml slurry) or anti-m^6A rabbit polyclonal antibody (Synaptic Systems, 30 μg antibody/ml slurry) for 3 hr at 4°C, respectively. Beads were then washed by five cycles of re-suspension with >2 volumes of buffer, then centrifugation (700 × *g*, 4°C for 2 min). The final 50% beads-antibody conjugate slurry was then aliquoted into 1.5 ml tubes, ~100 μl/tubes; tubes were centrifuged at 700 × *g*, 4°C for 2 min and beads (~50 μl) were resuspended with the RNA supernatant from the previous step and incubated at 4°C overnight in a tube rotator, with 0.5 μM random decamers (Invitrogen, Japan) in IPP buffer as blocking reagent. The tubes were then centrifuged at 700 × *g*, 4°C for 2 min; supernatant (unmethylated RNA) was transferred to a new tube, brought to 250 μl with the same buffer, and homogenized with 750 μl Sepasol RNA II Super by vortexing at full speed then kept at −80°C until processed further. Pellet (methylated RNA) were washed by five cycles of resuspension with at least 10 volumes of IPP buffer and centrifugation at 700 × *g*, 4°C for 2 min. The final pellet (~50 μl) was homogenized with 1 ml Sepasol RNA I super G by vortexing at full speed then kept at −80°C until processed further. Total RNA from the supernatant and pellet fractions was extracted with a combination of Qiazol/RNeasy micro kit following QIAGEN protocol, with Sepasol instead of Qiazol. The RNA eluate (~14 μl) was then used for RNA quantification by Nanodrop and reverse-transcribed using VILO. The specificity of our immunoprecipitation procedure on unfragmented RNA is demonstrated in Figure S3E.

Quantitative Real-Time PCR

Quantitative real-time PCR was performed using Platinum SYBR Green (Invitrogen) in StepOnePlus (Applied Biosystems, Tokyo, Japan). Quantification standards for each target cDNA were obtained using band-purified PCR products as templates. Data were normalized using relative expression of the housekeeping gene 36b4, which was found unaffected by either DAA treatment or *Mettl3* knockdown. Primer sequences given Table S2.

Western Blot

Cells were lysed directly with 300 μl 2× Laemmli buffer and boiled at 95°C for 10 min, then centrifuged at 14,000 g, 4°C for 10 min. Standard western blot procedures were performed using reagents from ATTO. Blotting membranes were revealed with ECL-prime (GE Healthcare) and visualized using a digital imaging system (LAS4000, Fujifilm).

Pulse-Chase Click RNA Cytochemistry

The Click-iT RNA Alexa Fluor 594 Imaging Kit was used according to manufacturer's protocol (Invitrogen). Cells were incubated for 2 hr with 1.5 mM ethynyl uridine and 200 nM dexamethasone for simultaneous synchronization, then medium was replaced with medium containing 0 or 100 μM DAA. Cells were fixed at the indicated chase time. For pulse-chase of siRNA-transfected cells, the labeling was also performed for 2 hr, simultaneously with dexamethasone shock, and terminated upon medium replacement.

Cellular Fractionation

Cells cultivated in 6-well plates were washed once in the dish with ice-cold PBS, 1 mM EDTA, then scraped on ice with 250 μl homogenization buffer (HB) at 4°C. Cells were transferred to a precooled 1.5 ml tube and cell walls were disrupted using 10 passages with a 25G needle, on ice. Cells were centrifuged at 700 × *g* for 10 min at 4°C, the supernatant (containing cytoplasmic RNA) carefully removed and transferred to a new tube on ice, its volume brought up to 250 μl with HB and immediately homogenized with 750 μl Sepasol RNA II Super by full-speed vortexing. The pellet was resuspended in 50 μl HB and layered on top of a 24% sucrose cushion HB. Nuclei were then centrifuged at 20,000 × *g* for 10 min at 4°C. The supernatant was discarded and nuclei were homogenized in 1 ml Sepasol RNA I Super G by full-speed vortexing, then incubated at 65°C, vortexing frequently until fully homogenized. RNA was then extracted, retro-transcribed and quantified following standard procedures.

Statistical Analyses

Statistical analyses and plots were performed with GraphPad prism 5, using statistical test proper for each figure, as indicated. Period estimates from all luminescence traces were obtained using BRASS on normalized data (Plautz et al., 1997).

SUPPLEMENTAL INFORMATION

Supplemental Information includes Extended Experimental Procedures, seven figures, and two tables and can be found with this article online at http://dx.doi.org/10.1016/j.cell.2013.10.026.

AUTHOR CONTRIBUTIONS

J.M.F., H.O. and M.D. designed the research; J.M.F., Y.Y., H.H., M.S.M., T.I., I.M., S.N., H.K. M.Y. performed the experiments. J.M.F. and H.O. wrote the manuscript.

ACKNOWLEDGMENTS

We thank Satchin Panda from the Salk Institute for the kind gift of U2OS Arntl-luc cells. This work was supported by Grant-in-Aid for Specially Promoted Research from the Ministry of Education, Culture, Sports, Science and Technology of Japan; by grants from JSPS (24111526, 24240058, and 25560426), SRF, and the Takeda Science Foundation (to H.O.). This work was also supported by the Funding Program for Next Generation World-Leading Researchers (NEXT program) from the JSPS (to M.D.) and by Grants-in-Aid for Scientific Research from the JSPS (23390203) (to I.M).

Received: June 5, 2013
Revised: August 16, 2013
Accepted: October 17, 2013
Published: November 7, 2013

REFERENCES

Akhtar, R.A., Reddy, A.B., Maywood, E.S., Clayton, J.D., King, V.M., Smith, A.G., Gant, T.W., Hastings, M.H., and Kyriacou, C.P. (2002). Circadian cycling of the mouse liver transcriptome, as revealed by cDNA microarray, is driven by the suprachiasmatic nucleus. Curr. Biol. *12*, 540–550.

Asher, G., Gatfield, D., Stratmann, M., Reinke, H., Dibner, C., Kreppel, F., Mostoslavsky, R., Alt, F.W., and Schibler, U. (2008). SIRT1 regulates circadian clock gene expression through PER2 deacetylation. Cell *134*, 317–328.

Audic, S., and Claverie, J.M. (1997). The significance of digital gene expression profiles. Genome Res. *7*, 986–995.

Backlund, P.S., Jr., Carotti, D., and Cantoni, G.L. (1986). Effects of the S-adenosylhomocysteine hydrolase inhibitors 3-deazaadenosine and 3-deazaaristeromycin on RNA methylation and synthesis. Eur. J. Biochem. *160*, 245–251.

Bujnicki, J.M., Feder, M., Radlinska, M., and Blumenthal, R.M. (2002). Structure prediction and phylogenetic analysis of a functionally diverse family of proteins homologous to the MT-A70 subunit of the human mRNA:m(6)A methyltransferase. J. Mol. Evol. *55*, 431–444.

Carmel, R., and Jacobsen, D.W. (2001). Homocysteine in health and disease (Cambridge: Cambridge University Press).

Carmody, S.R., and Wente, S.R. (2009). mRNA nuclear export at a glance. J. Cell Sci. *122*, 1933–1937.

Chen, R., Schirmer, A., Lee, Y., Lee, H., Kumar, V., Yoo, S.H., Takahashi, J.S., and Lee, C. (2009). Rhythmic PER abundance defines a critical nodal point for negative feedback within the circadian clock mechanism. Mol. Cell *36*, 417–430.

Chiang, P.K. (1998). Biological effects of inhibitors of S-adenosylhomocysteine hydrolase. Pharmacol. Ther. *77*, 115–134.

Clancy, M.J., Shambaugh, M.E., Timpte, C.S., and Bokar, J.A. (2002). Induction of sporulation in Saccharomyces cerevisiae leads to the formation of N6-methyladenosine in mRNA: a potential mechanism for the activity of the IME4 gene. Nucleic Acids Res. *30*, 4509–4518.

Cole, M.D., and Cowling, V.H. (2009). Specific regulation of mRNA cap methylation by the c-Myc and E2F1 transcription factors. Oncogene *28*, 1169–1175.

Cowling, V.H. (2010). Myc up-regulates formation of the mRNA methyl cap. Biochem. Soc. Trans. *38*, 1598–1601.

Dibner, C., Sage, D., Unser, M., Bauer, C., d'Eysmond, T., Naef, F., and Schibler, U. (2009). Circadian gene expression is resilient to large fluctuations in overall transcription rates. EMBO J. *28*, 123–134.

Doi, M., Ishida, A., Miyake, A., Sato, M., Komatsu, R., Yamazaki, F., Kimura, I., Tsuchiya, S., Kori, H., Seo, K., et al. (2011). Circadian regulation of intracellular G-protein signalling mediates intercellular synchrony and rhythmicity in the suprachiasmatic nucleus. Nat. Commun. *2*, 327.

Dominissini, D., Moshitch-Moshkovitz, S., Schwartz, S., Salmon-Divon, M., Ungar, L., Osenberg, S., Cesarkas, K., Jacob-Hirsch, J., Amariglio, N., Kupiec, M., et al. (2012). Topology of the human and mouse m6A RNA methylomes revealed by m6A-seq. Nature *485*, 201–206.

Eckel-Mahan, K.L., Patel, V.R., Mohney, R.P., Vignola, K.S., Baldi, P., and Sassone-Corsi, P. (2012). Coordination of the transcriptome and metabolome by the circadian clock. Proc. Natl. Acad. Sci. USA *109*, 5541–5546.

Eden, E., Lipson, D., Yogev, S., and Yakhini, Z. (2007). Discovering motifs in ranked lists of DNA sequences. PLoS Comput. Biol. *3*, e39.

Eden, E., Navon, R., Steinfeld, I., Lipson, D., and Yakhini, Z. (2009). GOrilla: a tool for discovery and visualization of enriched GO terms in ranked gene lists. BMC Bioinformatics *10*, 48.

Fernandez-Sanchez, M.E., Gonatopoulos-Pournatzis, T., Preston, G., Lawlor, M.A., and Cowling, V.H. (2009). S-adenosyl homocysteine hydrolase is required for Myc-induced mRNA cap methylation, protein synthesis, and cell proliferation. Mol. Cell. Biol. *29*, 6182–6191.

Jia, G., Fu, Y., Zhao, X., Dai, Q., Zheng, G., Yang, Y., Yi, C., Lindahl, T., Pan, T., Yang, Y.G., and He, C. (2011). N6-methyladenosine in nuclear RNA is a major substrate of the obesity-associated FTO. Nat. Chem. Biol. *7*, 885–887.

Jiao, X., Chang, J.H., Kilic, T., Tong, L., and Kiledjian, M. (2013). A mammalian pre-mRNA 5′ end capping quality control mechanism and an unexpected link of capping to pre-mRNA processing. Mol. Cell *50*, 104–115.

Kaida, D., Motoyoshi, H., Tashiro, E., Nojima, T., Hagiwara, M., Ishigami, K., Watanabe, H., Kitahara, T., Yoshida, T., Nakajima, H., et al. (2007). Spliceostatin A targets SF3b and inhibits both splicing and nuclear retention of pre-mRNA. Nat. Chem. Biol. *3*, 576–583.

Katada, S., and Sassone-Corsi, P. (2010). The histone methyltransferase MLL1 permits the oscillation of circadian gene expression. Nat. Struct. Mol. Biol. *17*, 1414–1421.

Koike, N., Yoo, S.H., Huang, H.C., Kumar, V., Lee, C., Kim, T.K., and Takahashi, J.S. (2012). Transcriptional architecture and chromatin landscape of the core circadian clock in mammals. Science *338*, 349–354.

Meyer, K.D., Saletore, Y., Zumbo, P., Elemento, O., Mason, C.E., and Jaffrey, S.R. (2012). Comprehensive analysis of mRNA methylation reveals enrichment in 3′ UTRs and near stop codons. Cell *149*, 1635–1646.

Miyazaki, K., Wakabayashi, M., Chikahisa, S., Sei, H., and Ishida, N. (2007). PER2 controls circadian periods through nuclear localization in the suprachiasmatic nucleus. Genes Cells *12*, 1225–1234.

Nakahata, Y., Kaluzova, M., Grimaldi, B., Sahar, S., Hirayama, J., Chen, D., Guarente, L.P., and Sassone-Corsi, P. (2008). The NAD+-dependent deacetylase SIRT1 modulates CLOCK-mediated chromatin remodeling and circadian control. Cell *134*, 329–340.

Plautz, J.D., Straume, M., Stanewsky, R., Jamison, C.F., Brandes, C., Dowse, H.B., Hall, J.C., and Kay, S.A. (1997). Quantitative analysis of Drosophila period gene transcription in living animals. J. Biol. Rhythms *12*, 204–217.

Quinlan, A.R., and Hall, I.M. (2010). BEDTools: a flexible suite of utilities for comparing genomic features. Bioinformatics *26*, 841–842.

Ripperger, J.A., and Merrow, M. (2011). Perfect timing: epigenetic regulation of the circadian clock. FEBS Lett. *585*, 1406–1411.

Robinson, M.D., and Smyth, G.K. (2007). Moderated statistical tests for assessing differences in tag abundance. Bioinformatics *23*, 2881–2887.

Rosbash, M. (1995). Molecular control of circadian rhythms. Curr. Opin. Genet. Dev. *5*, 662–668.

Schalinske, K.L., and Steele, R.D. (1992). Variations in S-adenosylmethionine, S-adenosylhomocysteine and adenosine concentrations in rat liver. Biofactors *3*, 265–268.

Trapnell, C., Pachter, L., and Salzberg, S.L. (2009). TopHat: discovering splice junctions with RNA-Seq. Bioinformatics *25*, 1105–1111.

Valekunja, U.K., Edgar, R.S., Oklejewicz, M., van der Horst, G.T., O'Neill, J.S., Tamanini, F., Turner, D.J., and Reddy, A.B. (2013). Histone methyltransferase MLL3 contributes to genome-scale circadian transcription. Proc. Natl. Acad. Sci. USA *110*, 1554–1559.

Vollmers, C., Schmitz, R.J., Nathanson, J., Yeo, G., Ecker, J.R., and Panda, S. (2012). Circadian oscillations of protein-coding and regulatory RNAs in a highly dynamic mammalian liver epigenome. Cell Metab. *16*, 833–845.

Wilkins, A.K., Barton, P.I., and Tidor, B. (2007). The Per2 negative feedback loop sets the period in the mammalian circadian clock mechanism. PLoS Comput. Biol. *3*, e242.

Woo, K.C., Kim, T.D., Lee, K.H., Kim, D.Y., Kim, W., Lee, K.Y., and Kim, K.T. (2009). Mouse period 2 mRNA circadian oscillation is modulated by PTB-mediated rhythmic mRNA degradation. Nucleic Acids Res. *37*, 26–37.

Yamaguchi, S., Mitsui, S., Miyake, S., Yan, L., Onishi, H., Yagita, K., Suzuki, M., Shibata, S., Kobayashi, M., and Okamura, H. (2000). The 5′ upstream region of mPer1 gene contains two promoters and is responsible for circadian oscillation. Curr. Biol. *10*, 873–876.

Yoo, S.H., Yamazaki, S., Lowrey, P.L., Shimomura, K., Ko, C.H., Buhr, E.D., Siepka, S.M., Hong, H.K., Oh, W.J., Yoo, O.J., et al. (2004). PERIOD2: LUCIFERASE real-time reporting of circadian dynamics reveals persistent circadian oscillations in mouse peripheral tissues. Proc. Natl. Acad. Sci. USA *101*, 5339–5346.

Zhang, E.E., Liu, A.C., Hirota, T., Miraglia, L.J., Welch, G., Pongsawakul, P.Y., Liu, X., Atwood, A., Huss, J.W., 3rd, Janes, J., et al. (2009). A genome-wide RNAi screen for modifiers of the circadian clock in human cells. Cell *139*, 199–210.

Zheng, G., Dahl, J.A., Niu, Y., Fedorcsak, P., Huang, C.M., Li, C.J., Vågbø, C.B., Shi, Y., Wang, W.L., Song, S.H., et al. (2013). ALKBH5 is a mammalian RNA demethylase that impacts RNA metabolism and mouse fertility. Mol. Cell *49*, 18–29.